ORIGINAL PAPER

RJME
Romanian Journal of Morphology & Embryology
http://www.rjme.ro/

Spatiotemporal expression of extracellular matrix components during the chondrogenic and osteogenic phases of bone healing

MOYSES MESSIAS SOUZA DE SANT'ANNA[1)], LUIZ ALBERTO BATISTA[2)], THAÍS CRISTINA MENDES DA SILVA[1)], LISZT PALMEIRA OLIVEIRA[3)], JORGE JOSÉ DE CARVALHO[1)]

[1)]*Laboratory of Ultrastructure and Tissue Biology, Department of Histology and Embryology, State University of Rio de Janeiro (UERJ), Brazil*

[2)]*Laboratory of Biomechanics and Motor Behavior, Institute of Physical Education and Sports, State University of Rio de Janeiro (UERJ), Brazil*

[3)]*Laboratory of Microsurgery, Department of Surgical Specialties, Faculty of Medical Sciences, State University of Rio de Janeiro (UERJ), Brazil*

Abstract

In this study, we investigated the cascade of events involved in the early phases of bone healing in rats, especially the transition from chondrogenesis to osteogenesis, which involves cellular and extracellular matrix (ECM) components. We used a standardized closed tibial fracture model in Wistar rats, which was divided into nine groups of five animals each, and the fracture area was evaluated at 0, 12, 24, 48, 72, 96, 144, 192, and 240 hours post-injury. Histological, histochemical, immunohistochemical and morphometric techniques were used to evaluate the proliferating cell nuclear antigen (PCNA), transforming growth factor-beta (TGF-*β*), vascular endothelial growth factor (VEGF), type I procollagen (procoll-I), type I collagen (coll-I), and type II collagen (coll-II) expression at every time point. TGF-*β* expression peaked after 144 hours, in the initial chondrogenic phase. VEGF expression reached the first peak at 96–144 hours post-injury, in the initial chondrogenic phase and the second peak at 240 hours, in the osteogenic phase. Except at 48 hours, PCNA expression increased gradually from 12 hours and peaked at 96 hours in the prechondrogenic phase, and then decreased gradually until 240 hours in the osteogenic phase. Total collagen (T-coll) and coll-II reached an expression peak at 144 hours, in the chondrogenic phase. No differences were observed between their expression from 12 hours to 72 hours and at 240 hours post-injury. The results suggest that spatiotemporal expression of ECM components during the chondrogenic and osteogenic phases of bone healing depends on several combined and orchestrated factors. A better understanding of the coordinated participation of cells and ECM components in the early bone healing process may provide new insights into the etiology of abnormal or delayed fracture healing.

Keywords: bone healing, extracellular matrix, chondrogenic and osteogenic phases, standardized fracture.

Introduction

Morbidity associated with complications arising from the bone healing process in young and ageing adults represents an important public health problem, with social and economic implications [1–3]. Thus, understanding of the biological mechanisms involved in bone fractures, bone remodeling, and bone diseases has been the subject of intense investigation [4–6].

Although bone repair processes have been widely investigated in an attempt to create new therapies to accelerate fracture healing [7, 8], the mechanisms of action of cells and extracellular matrix (ECM) components during the chondrogenic and osteogenic phases of endochondral fracture healing are not fully understood. Specifically, whether chondroblasts and osteoblasts are derived from distinct lineages of precursor cells or whether chondroblasts change their phenotype into bone-forming cells during the transition from the chondrogenic to the osteogenic phase remains controversial [9, 10]. A number of molecular mediators and cells interact *via* different pathways. Even considering the involvement of many local and systemic factors, failure of naturally occurring mechanisms can occur and lead to either delayed consolidation or no consolidation.

To shed light on this issue, in this study, we used a standardized closed tibial fracture model in rats to investigate the cascade of events involved in the early phases of bone healing, with emphasis on the transition stage from chondrogenesis to osteogenesis, which involves cells and ECM components. Histological, histochemical, immunohistochemical and morphometric techniques were applied to evaluate the proliferating cell nuclear antigen (PCNA), transforming growth factor-beta (TGF-*β*), vascular endothelial growth factor (VEGF), type I procollagen (procoll-I), type I collagen (coll-I), and type II collagen (coll-II) and total collagen (T-coll) expression.

Materials and Methods

Animal model

The procedures adopted in this study are in accordance with the ethical principles for animal experimentation adopted by the *Brazilian College of Animal Experimentation* (COBEA) and were approved by the Animal Ethics Committee of the Roberto Alcantara Gomes (IBRAG)

Institute of Biology of the State University of Rio de Janeiro (UERJ), Brazil (CEA/167/2006).

Our sample consisted of 45 male Wistar rats, aged three months, with an average weight of 300 g. For the experimental group, fractures were induced in animals' right hind legs, and animals without any intervention served as a control group. Animals were divided into nine groups (n=5 each) that were analyzed at different time points prior to injury [represented by zero (0)] and 12, 24, 48, 72, 96, 144, 192, and 240 hours post-injury. Animals were euthanized in a CO_2 chamber.

Images were obtained with an optical microscope (Olympus© BX51 model and an Olympus© DP70 camera) coupled to a personal computer, and confocal laser scanning microscopy (model LSM 510, Carl Zeiss) was used to evaluate the distribution of coll-II, procoll-I, and coll-I. Double staining was performed with Alexa Fluor® 488 for coll-I (green), and Alexa Fluor® 555 for procoll-I (red) [11].

Three histology slides from longitudinal sections of the tibial diaphysis were selected from each animal, and three microscope fields were evaluated from each slide, as represented by the squares in Figure 3h, for morphometric analysis of the total fracture area: one square containing the bone marrow, and the other two squares containing both sides of the bone diaphysis.

All phases of bone healing, from 12 hours to 240 hours post-injury, were qualitatively and quantitatively analyzed, focusing on the chondrogenic and osteogenic stages, *i.e.*, between 96 hours and 240 hours.

Fracture model

The animals were anaesthetized with 0.1 mL/100 g intraperitoneal Thiopental (EIFG Chemicals, Hong Kong). Prior to the fracture, an intramedullary fixation was performed with a modified access route. With the knee in flexion, percutaneous access was made *via* the patellar tendon, and a Kirschner wire (0.6 mm in diameter and 2 cm in length) was carefully introduced into the intramedullary canal of the tibia at the insertion site of the anterior cruciate ligament until its stabilization in the distal end of the medullary canal. The wire was cut close to the tibial plateau in such a manner that the knee extension was not hindered. No suture was needed [12, 13].

After this, fractures were induced in the diaphysis of the right tibia by means of a standardized fracture device (Figure 1), which was constructed according to the system described by An *et al.* [14], with modifications that allowed less soft tissue damage. The instrument used consisted of five parts: a framework, a base for supporting the animal, a guillotine with a blunt tip, a weight of 250 g, and a spring system (Figure 1). The tibial diaphysis was positioned at the base of the instrument, below the guillotine.

In a previous pilot study, weights of 100 to 250 g were dropped from a height of 30 cm to determine the best weight and height to use to induce the fracture, and we selected 250 g. Instrument calibration was obtained by comparing the values for strength, speed, power, and distance.

Fractures were evaluated with simple lateral X-rays (Figure 2). Each image was evaluated three times by the same observer, with at least a one-week interval between evaluations, using Müller's fracture classification (AO – *Association for Ostheosynthesis*), which categorizes nine types of fractures, including simple and complex [15]. Transverse (Figure 2a) and short oblique fractures (Figure 2b) constitute the subgroup of simple fractures, while irregular (Figure 2c) and segmental fractures (Figure 2d) make up the complex fracture subgroup. However, only the transverse fractures were selected in the present study.

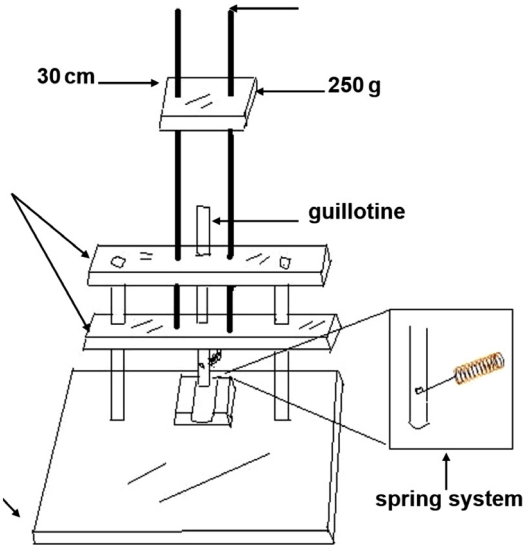

Figure 1 – ***Schematic representation of the device used to produce standardized closed experimental fractures, adapted from the system described by An et al. (1994) [14].***

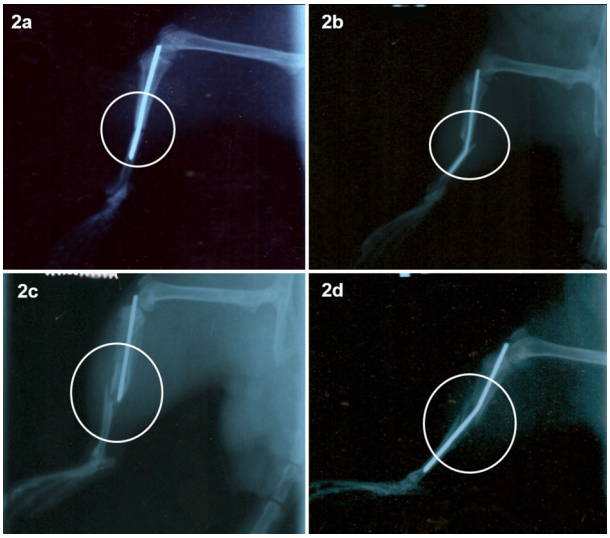

Figure 2 – ***X-ray image of tibial fractures: (a) Transverse tibial fracture induced in the study; (b) Short oblique fracture; (c) Irregular fracture; (d) Segmental fracture.***

Histology, histochemistry and immunohistochemistry

The tibia was removed in such a manner as to preserve the soft tissues and keep the fracture line in the middle third of the tibia. The hind limbs were dissected and fixed with glutaraldehyde and paraformaldehyde solution, for two days [16]. After being fixed, the samples were

decalcified with 8% ethylenediaminetetracetic acid (EDTA), for three weeks, to better preserve tissue structures. The solution was changed daily, and tissue softness was tested with a fine-tipped needle without damaging the region of the fracture. The samples were embedded in paraffin, and longitudinal 4-μm-thick sections were obtained. The samples were stained with Hematoxylin and Eosin (HE) and Masson's trichrome. Immunoperoxidase staining for TGF-β (sc-146; rabbit polyclonal), VEGF (sc-7269; mouse monoclonal), PCNA (sc-56; mouse monoclonal), and coll-II (sc-7764; goat polyclonal) and immunofluorescence with co-staining for procoll-I (sc-30136; rabbit polyclonal) and coll-I (sc-8788; goat polyclonal) was performed. In addition, immunofluorescence staining for coll-II was performed. To verify staining specificity, a negative control was included in each staining run. All antibodies used were from Santa Cruz Biotechnology (Santa Cruz, CA, USA). Histochemistry for T-coll was performed using Picrosirius Red (PSR) staining visualized with polarized light microscopy. ECM components were detected by immunoperoxidase staining, as previously described [17].

Procedure

Sections from formalin-fixed, paraffin-embedded tissues were deparaffinized in the following sequence: store at 58ºC (5 minutes), deparaffinize and hydrate to distilled water (xylene 1, 2 and 3, at 3 minutes each); alcohol 100%, 90% and 70% (3 minutes each); distilled water (3 minutes), moist chamber, hydrogen peroxide (15 minutes), rinse with water (wash bottle), phosphate-buffered saline (PBS, 3×5 minutes), citrate buffer pH 6, at 96ºC (20 minutes) for antigenic recovery, PBS (3×5 minutes), PBS/bovine serum albumin (BSA) 3% (20 minutes), primary antibody overnight, PBS (3×5 minutes), secondary biotinylated antibody (LSAB2 kit or Invitrogen for one hour), PBS (3×5 minutes), Streptavidin (30 minutes), 3,3-Diaminobenzidine (DAB) (15 seconds to one minute), distilled water (2 minutes), Hematoxylin (one minute), distilled water (2 minutes), dehydrated alcohol 70%, 90% and 100%, xylene 1, 2, 3 for 3 minutes each), covered with epoxy resin.

The protocol for immunofluorescence staining was similar to that for peroxidase, with the exception of the double labeling and the mounting.

Morphometric and statistical analysis

VEGF, TGF-β, PCNA, coll-II, and T-coll were analyzed by morphometry. An interactive color segmentation method was employed for morphometric analysis using Image-Pro Plus® software (Media Cybernetics, Inc., Rockville, MD, USA), ver. 7.0. As quantitative scientific instruments, computer image analysis systems have the ability to perform automatically repeated tasks efficiently and tirelessly. It is the task of scientific image analysis to mimic the superior qualitative abilities of human visual analysis and extend this ability to quantitative measurements.

The equipment and requirements for use of the system were a Windows 7 Pro & Ultimate 32-bit or 64-bit operating system; 40 GB of free disk space; a processor with 2.1 GHz and 4 GB of RAM, and a Dell 24 Gaming monitor S2417DG. The entire system was coupled to an optical microscope (Olympus© BX51 model and an Olympus© DP70 camera).

The method consists of five basic steps:

(*a*) Image input: accurate image analysis began with acquisition of previously selected images;

(*b*) Image calibration: a wide range of morphological filters were used to precisely segment structures and prepare images for automatic segmentation and measurement;

(*c*) Image segmentation: red, green and blue (RGB) pseudo-color was used to highlight features of interest in a grey scale image according to the specific staining for each structure. Colors were used to visually amplify specific intensities that are normally difficult to distinguish from their surroundings;

(*d*) Object counting and measurement: counting and characterization of the morphological structures were performed using over 50 manual and automatic measurement tools to assess areas, perimeters, lengths, roundness, major and minor axes, angles, centroids, holes, and population density and, in our case, cells and ECM;

(*e*) Data analysis: counting of the population density according to the area of the morphological structures identified by the specific color was performed to generate a numerical table to facilitate statistical analysis.

Statistical analysis was performed using Prism software (Graph Pad Inc., USA), ver. 5.2. A Kruskal–Wallis test was used to analyze non-parametric samples. Groups were compared using Dunn's multiple comparison test. *P*-values <0.05 were considered statistically significant.

Results

Fracture classification

We observed that 250 g of weight falling from a 30 cm height was sufficient to induce a transverse tibial fracture. The fracture analysis method (AO) was precisely for standardization of induced fractures. In this case, the transverse fracture was the one with the highest percentage compared with other fractures. Tibial fractures were evaluated with simple lateral radiographs. We found that 86% of the fractures were simple; of these, 68% were transverse and 18% were short oblique. Of the remaining 14% of fractures that were complex, 8% were irregular and 6% were segmental. However, as mentioned above, only the transverse fractures were selected for the present study.

Histological, histochemical and immunohistochemical results

Hematoxylin and Eosin

Analysis of images taken from 12 hours to 240 hours after injury revealed a large hematoma with a large number of platelets, leukocytes, and erythrocytes (Figure 3a), as well as bone fragments. At 24 hours post-injury, we observed bone fragments still surrounded by the fracture hematoma in one of the fracture edges, which helps maintain bone fragments close together to stabilize the callus (Figure 3b). At 48 hours post-injury, cells from the fracture hematoma were concentrated between the

bone fragments, and we observed periosteal thickening (Figure 3c). At 72 hours post-injury, periosteal cells were observed in the early callus between bone fragments (Figure 3d). After 96 hours, we observed a callus as a replacement tissue between fracture fragments, surrounded by muscle tissue, periosteum, and a smaller hematoma (Figure 3e). At 144 hours post-injury, the callus between fracture fragments was more consistent (Figure 3f), and at 192 hours, a fracture callus containing cartilage cells was formed between the fragments (Figure 3g). The callus was completely formed at 240 hours post-injury, confirming the classification of the fracture as transverse. The squares represent the images selected for morphometric and qualitative analysis (Figure 3h).

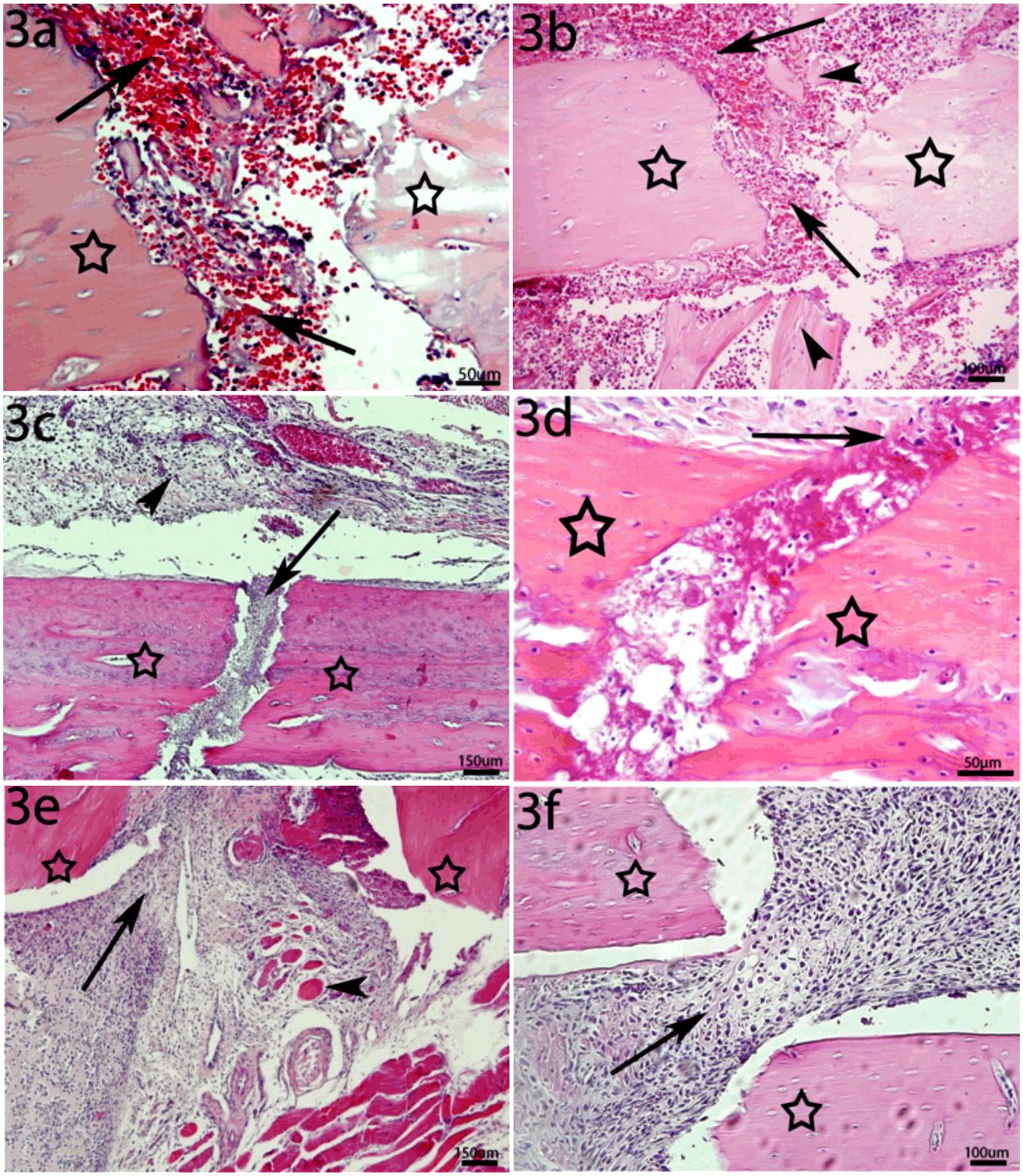

Figure 3 – ***Photomicrographs of transverse sections of bone fractures (HE staining): (a) At 12 hours post-injury, the hematoma area (arrows) between bone fragments (stars); (b) At 24 hours post-injury, bone fragments (arrowheads) near the fracture area between cortical bones (stars); (c) At 48 hours post-injury, the lateral edge of the fracture without deviation between bone fragments (stars) and thickened periosteum (vertical bar); (d) At 72 hours post-injury, the lateral edge of fractured cortical bone (arrow) between bone fragments (stars); (e) At 96 hours post-injury, the fracture centre (arrow) between the fragments (stars), surrounded by muscle tissue (arrowhead); (f) At 144 hours post-injury, cartilaginous tissue (arrow) between the fragments (star). HE: Hematoxylin–Eosin.***

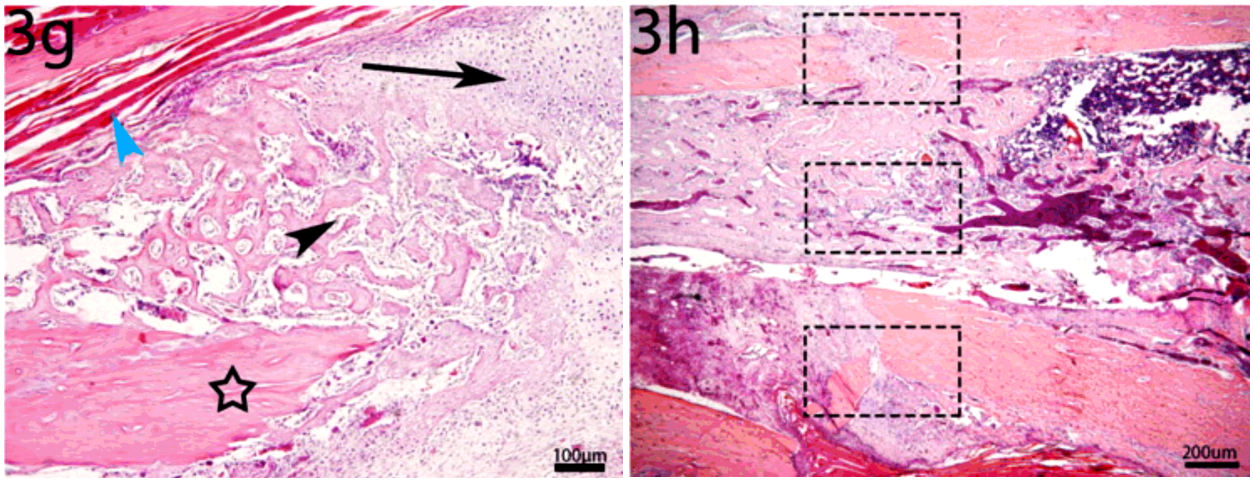

Figure 3 (continued) – ***Photomicrographs of transverse sections of bone fractures (HE staining): (g) At 192 hours post-injury, cartilage cells (arrow) and newly formed bone in the centre of the fracture (arrowhead) between cortical bone fragments (star), and muscle tissue on the lateral edge (arrowhead blue); (h) At 240 hours post-injury, the squares represent the images selected for morphometric analysis. HE: Hematoxylin–Eosin.***

Masson's trichrome

The histological slides from longitudinal sections of the tibial diaphysis stained with Masson's trichrome show the histological characteristics of the bone tissue, the integrity of compact bone on the top edge of the image, the bone marrow in the centre, and compact bone at the bottom edge (Figure 4a). Figure 4b shows an image of HE staining of the same region as the fracture in the control group.

At 96 hours post-injury, we observed early stage formation of a cartilaginous callus between the fracture fragments and a small fracture hematoma (Figure 4c). A high-magnification image (square area in Figure 4c) shows the centre of the fracture callus, where intense cell concentration and cellular reorganization in the fibrillar tissue can be observed (Figure 4d). At 144 hours post-injury, we observed the formation of a cartilaginous callus in the top edge of the fracture centre (Figure 4e). A high-magnification image (square area in Figure 4e) shows hypertrophic chondrocytes (Figure 4f). At 192 hours, we observed a smaller cartilaginous callus area and a larger hard callus area at the centre of the fracture (Figure 4g). A high-magnification image (square area in Figure 4f) shows a cartilaginous area and a hard callus area (Figure 4h). After 240 hours, we identified a hard callus formed in the areas adjacent to the fracture centre involving the bone fragment from the periosteum (Figure 4i). A high-magnification image (square area in Figure 4i) shows periosteum-derived cells forming the new bone (Figure 4j).

Transforming growth factor-beta

TGF-β labeling was observed in all stages of bone regeneration. However, the immunoreaction was more widely distributed in the ECM of the periosteum in the control group (Figure 5a). Twelve hours after injury, TGF-β staining was intense in the fracture hematoma (Figure 5b). After 144 hours, we observed the highest TGF-β expression, different patterns of distribution near the fracture, weak staining in the periosteum, and moderate staining in the chondrogenic and osteoid region (Figure 5c). After 240 hours, TGF-β was expressed on the edges of the gaps in the newly formed bone in the centre of the fracture (Figure 5d).

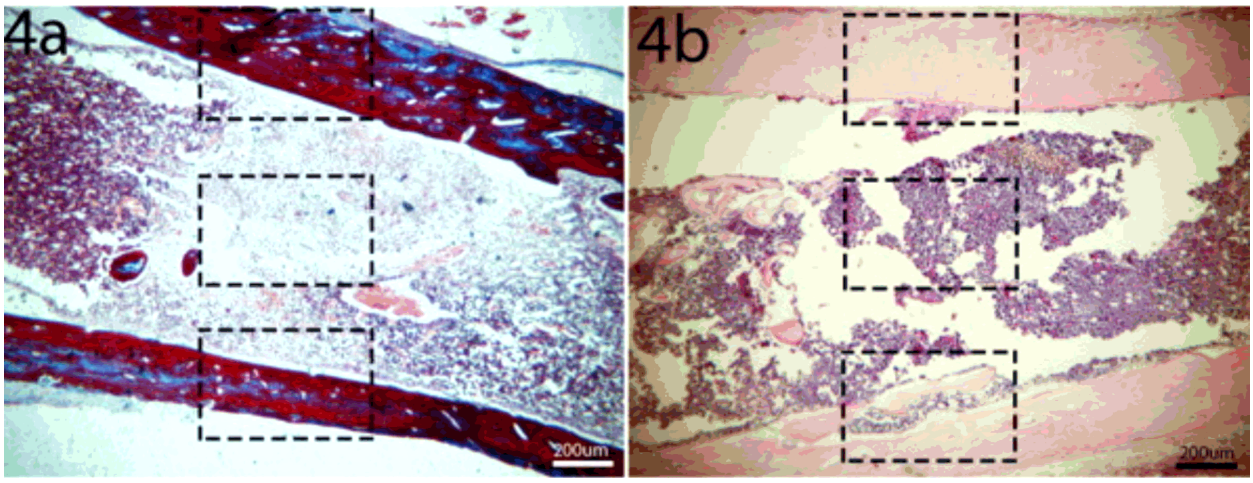

Figure 4 – ***Photomicrographs of transverse sections of bone fractures: (a) Control group, Masson's trichrome staining; (b) Control group, HE staining. The squares represent the images selected for qualitative and quantitative analysis. HE: Hematoxylin–Eosin.***

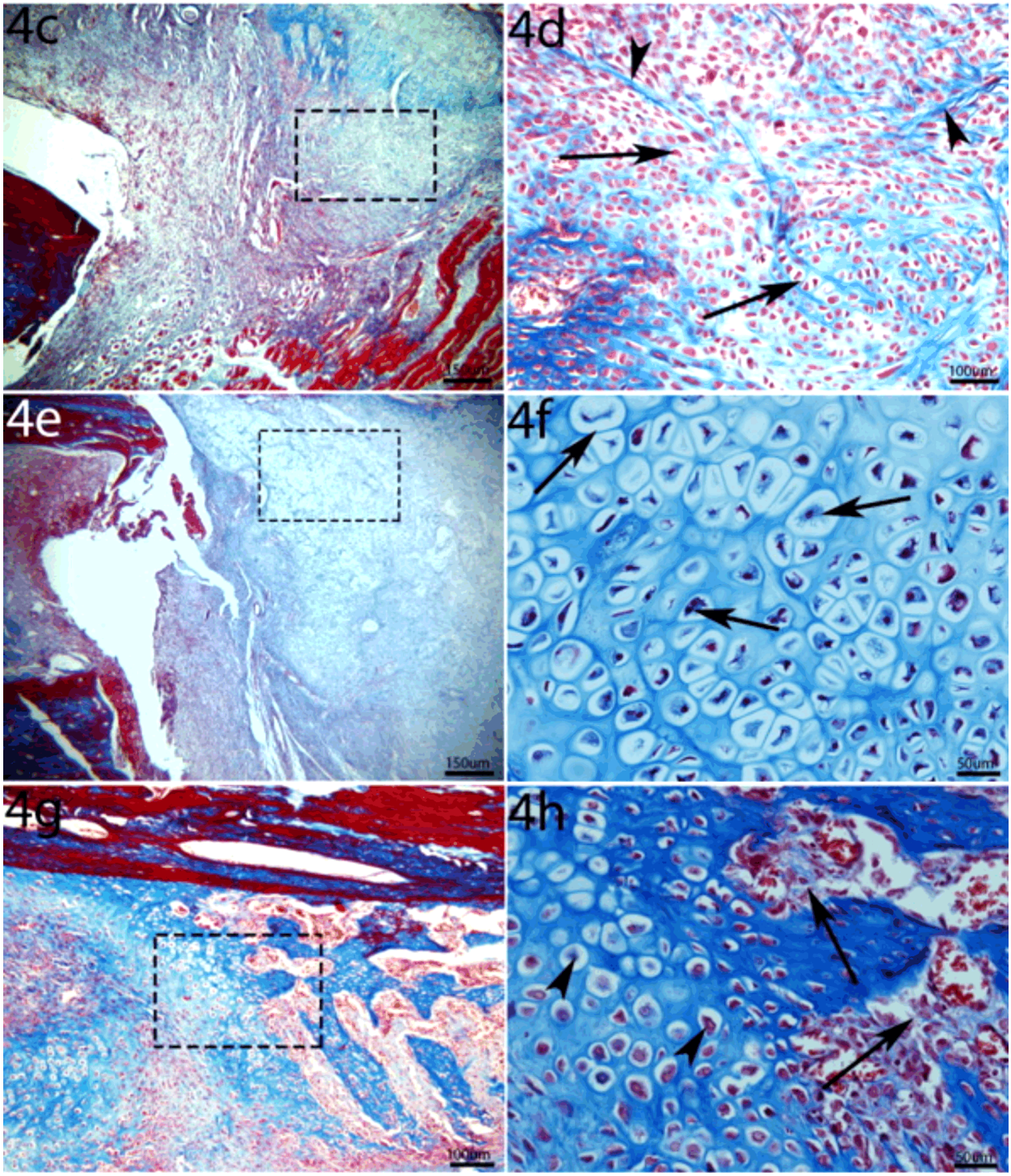

Figure 4 (continued) – ***Photomicrographs of transverse sections of bone fractures (Masson's trichrome staining): (c) At 96 hours post-injury, image selected for analysis; (d) High-magnification image of the area selected in (c) showing collagen fibers (arrowheads) and cartilaginous cells (arrows); (e) At 144 hours post-injury, image selected for analysis; (f) High-magnification image of the area selected in (e) showing a cartilaginous area containing hypertrophic chondrocytes (arrows); (g) At 192 hours post-injury, image selected for analysis; (h) High-magnification image of the area selected in (g) showing a cartilaginous area (arrowheads) and the formation of new bone in the same region (arrows). The squares represent the images selected for qualitative and quantitative analysis.***

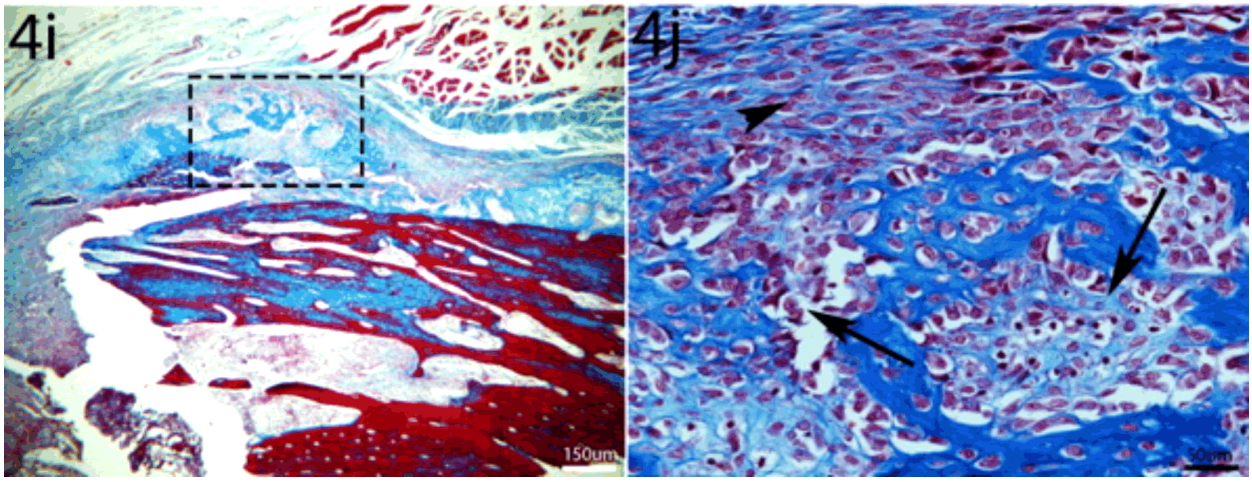

Figure 4 (continued) – ***Photomicrographs of transverse sections of bone fractures (Masson's trichrome staining): (i) At 240 hours post-injury, image selected for analysis (the square represent the image selected for qualitative and quantitative analysis); (j) High-magnification image of the area selected in (i) showing complete formation of the hard callus, osteogenic cells derived from the periosteum (arrowhead), and new bone formation (arrows).***

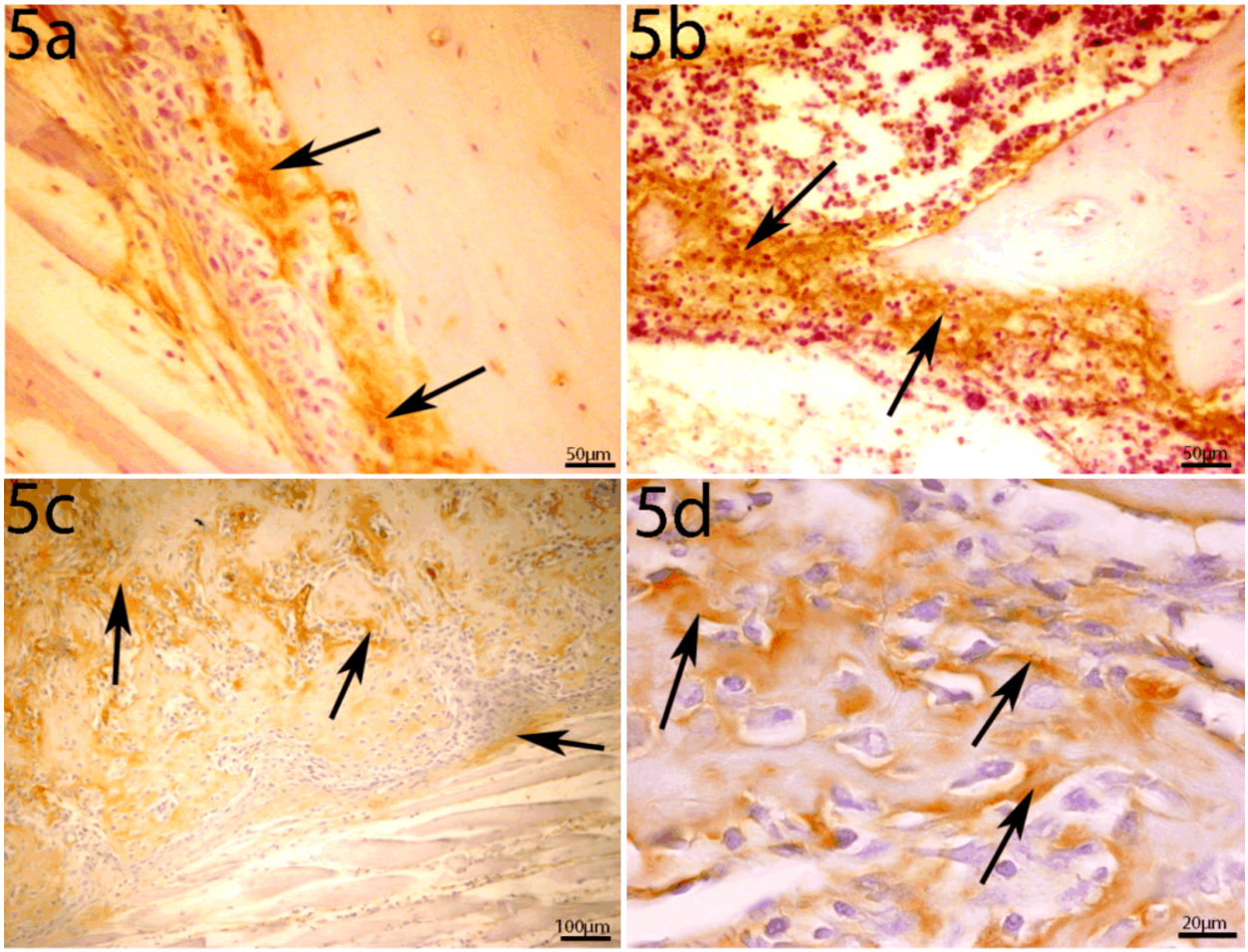

Figure 5 – ***Photomicrographs of transverse sections of bone fractures, showing immunoreaction for TGF-β: (a) Control group, TGF-β was identified in the ECM of the osteogenic periosteum (arrows); (b) At 12 hours post-injury, the hematoma area – observe the immunoreaction in the centre of the fracture (arrows); (c) At 144 hours post-injury, TGF-β labeling (arrows) in different regions near the fracture; (d) At 240 hours post-injury, TGF-β labeling at the edges of trabeculae in newly formed bone (arrows). TGF-β: Transforming growth factor-beta; ECM: Extracellular matrix.***

Vascular endothelial growth factor

At 12 hours post-injury, we observed VEGF immunoreactivity in the ECM in the centre of the fracture (Figure 6a). At 96 hours post-injury, VEGF was widely distributed in the thickened periosteum near the fracture (Figure 6b). At 144 hours post-injury, the VEGF immunoreaction revealed new vascularization between bone fragments (Figure 6c). After 240 hours, we observed intense staining at the edges of the new trabecular bone in the centre of the fracture (Figure 6d). In the control group, we identified VEGF immunoreaction in small vessels but did not observe any change in its distribution pattern.

Proliferating cell nuclear antigen

From 12 hours to 48 hours post-injury, the PCNA immunoreaction was weak in the central region of the fracture (not shown), while a strong immunoreaction was observed near the central region of the fracture after 72 hours (Figure 7a). After 96 hours, a large number of PCNA-positive cells migrated to the centre of the fracture from the osteogenic periosteum (Figure 7b). At 144 hours post-injury, PCNA immunoreaction was observed in the osteogenic periosteum and in some isogenic groups of cells. Hypertrophic chondrocytes were seen below the periosteum (Figure 7c). After 192 hours, the immunoreaction was less intense in the region close to the fracture, and a greater number of hypertrophic chondrocytes was observed (Figure 7d). The number of PCNA-positive cells decreased in the periosteum at 240 hours post-injury. In the control group, moderate immunostaining was observed in the thin periosteum (not shown).

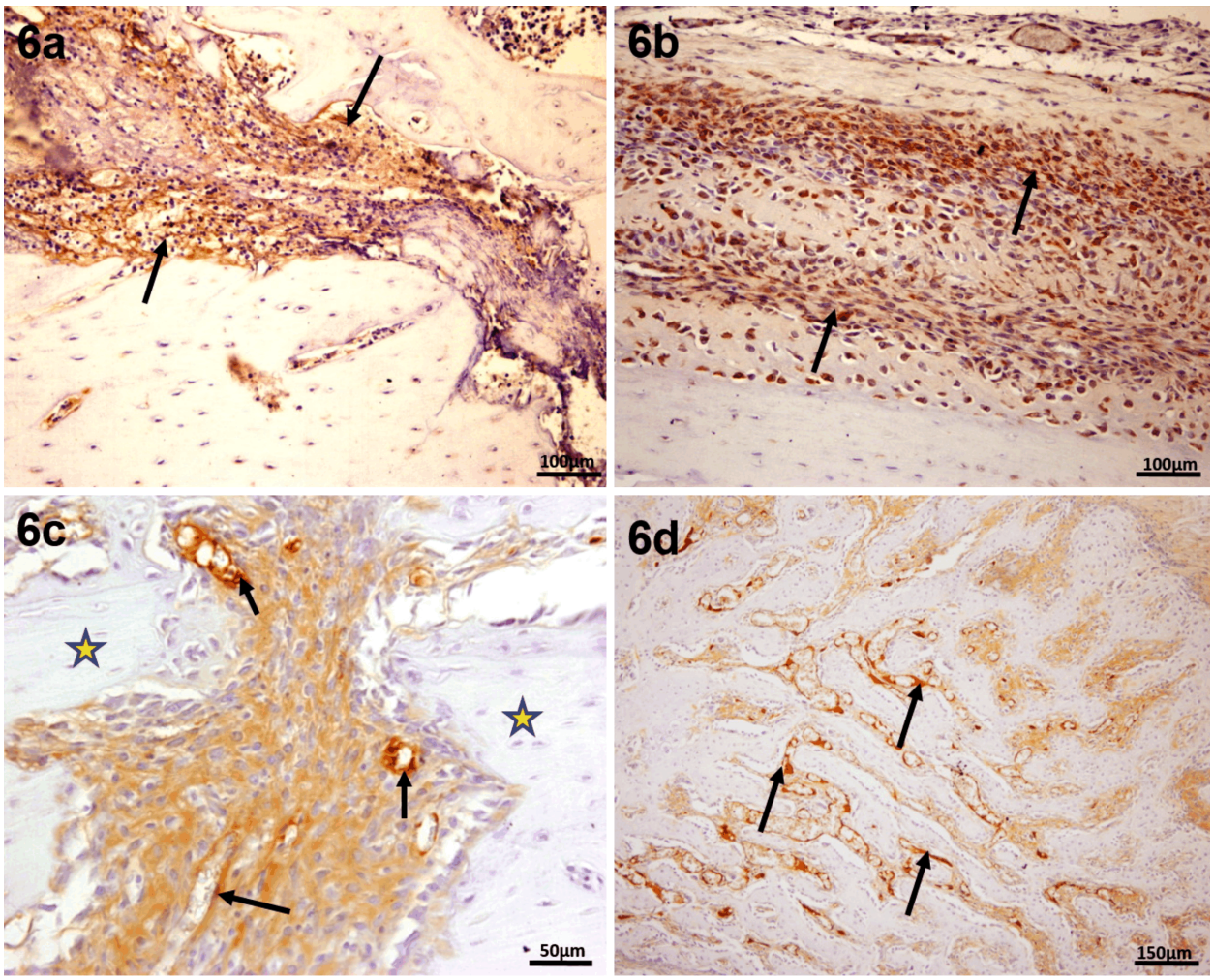

Figure 6 – ***Photomicrographs of transverse sections of a bone fracture showing immunoreaction for VEGF: (a) At 12 hours post-injury, VEGF labeling in the hematoma of the fracture (arrows); (b) At 96 hours post-injury, VEGF was identified in thickened periosteum near the fracture centre (arrows); (c) At 144 hours post-injury, new vascularization in the centre of the fracture (arrows) between bone fragments (stars); (d) At 240 hours post-injury, VEGF labeling in the edges of the newly formed trabecular bone (arrows). VEGF: Vascular endothelial growth factor.***

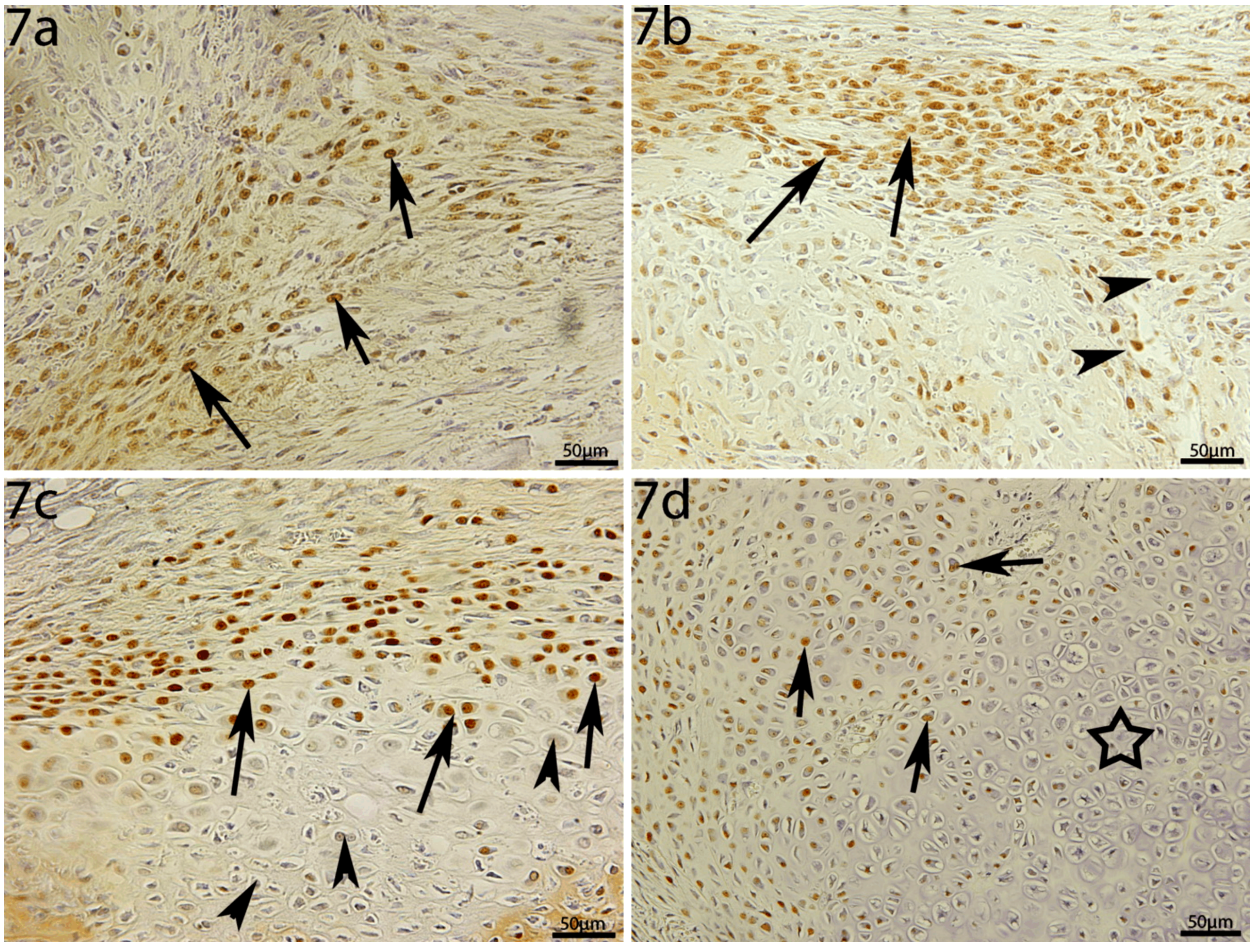

Figure 7 – ***Photomicrographs of transverse sections of a bone fracture, showing immunoreaction for PCNA: (a) At 72 hours post-injury, PCNA was identified near the central region of the fracture (arrows); (b) At 96 hours post-injury, PCNA labeling in the layer of periosteum near the fracture (arrows) – cells migrating to the centre of the fracture (arrowheads); (c) At 144 hours post-injury, PCNA was strongly expressed in the osteogenic periosteum (arrows) – hypertrophic chondrocytes are observed in the deeper layer (arrowheads); (d) At 192 hours post-injury, PCNA is more dispersed in the region close to the fracture (arrows) and in the region with high amounts of hypertrophic chondrocytes (star). PCNA: Proliferating cell nuclear antigen.***

Type II collagen

From 12 hours to 72 hours post-injury, small quantities of collagen were observed in the periosteum, near the fracture and in the central region of the fracture, as shown by coll-II immunostaining. However, at 96 hours post-injury, we observed a more intense immunostaining in thick periosteum near the fracture (Figure 8a). After 144 hours, a strong immunoreaction was seen in the ECM of the central region between fracture fragments (Figure 8b). At 192 hours post-injury, coll-II immunostaining was observed around hypertrophic chondrocytes, in the central region of the fracture, surrounded by an area of new bone formation, which characterized the formation of a cartilaginous callus (Figure 8c). After 240 hours, the immunoreaction was localized in the ECM surrounding chondrocytes in a small area in the central region of the fracture near the bone fragments (Figure 8d). Additionally, the quantity of coll-II decreased in the central region of the fracture 192 hours and 240 hours after the injury. In the control group, small vessels in the compact bone were also immunostained (not shown).

Confocal laser scanning microscopy analysis revealed that coll-II was present, as a green plot, in the osteogenic periosteum near the fracture site 96 hours after injury (Figure 9a). After 144 hours, more coll-II was expressed by chondrocytes, which grew distant from the periosteum towards the centre of the fracture (not shown). Moreover, compared to the previous time points, we observed the highest expression of coll-II by area. A chondrogenic area was seen around isogenic cell groups located in the central region of the fracture. At 240 hours post-injury, coll-II immunostaining was less intense in the ECM (Figure 9b). Chondrocytes were widely spaced, suggesting that they were moving away from the periosteum, and coll-II was more densely distributed in the ECM (not shown).

Type I collagen and type I procollagen

From 12 hours to 72 hours post-injury, a slight immunoreaction for coll-I (green) and procoll-I (red) was observed in the central region of the fracture (not shown). After 144 hours, we identified coll-I immunostaining in the ECM and discrete expression of procoll-I in cells adjacent to the central regions of the fracture, close to the periosteum. In the same region, we also identified the initial formation of small dark lacunae, isogenic groups of cells, and a layer of the periosteum

(Figure 9c). At 240 hours post-injury, coll-I immunostaining was more widely distributed in the ECM in the central region of the fracture and was more intense than that of coll-II. Procoll-I was detected intracellularly in the osteogenic area as well as in bone fragments (Figure 9d). At previous time points, coll-I immunostaining was less intense in the central region of the fracture, while coll-II predominated in this area at 144 hours and 192 hours post-injury.

Total collagen

PSR-stained histology sections were visualized under polarized light. At 96 hours post-injury, small quantities of collagen fibers (in red) were observed in the central region of the fracture (Figure 10, a and b). After 144 hours, we observed large collagen-stained areas in the central region of the fracture, as well as at the ends of bone fragments (Figure 10, c and d), which were smaller after 192 hours (Figure 10, e and f). At 240 hours post-injury, collagen staining was observed in the callus in the central region of the fracture and at trabecular edges of the new bone (Figure 10, g and h).

Quantitative analysis (morphometry)

Morphometric analysis of ECM components and cell proliferation showed that each component was maximally expressed (expression peak per area), at different time points after injury. Figure 11 shows the distribution of TGF-β, VEGF, PCNA, T-coll, and coll-II from 12 hours to 240 hours post-injury. TGF-β expression peaked after 144 hours, and no differences were observed at the other time points (Figure 11a). VEGF expression reached the first peak at 96–144 hours post-injury and the second peak at 240 hours (Figure 11b). Except at 48 hours, PCNA expression increased gradually from 12 hours to a peak at 96 hours and then decreased gradually until 240 hours (Figure 11c). T-coll and coll-II reached their expression peak at 144 hours. No differences were observed between their expression from 12 hours to 72 hours, and at 240 hours post-injury (Figure 11d).

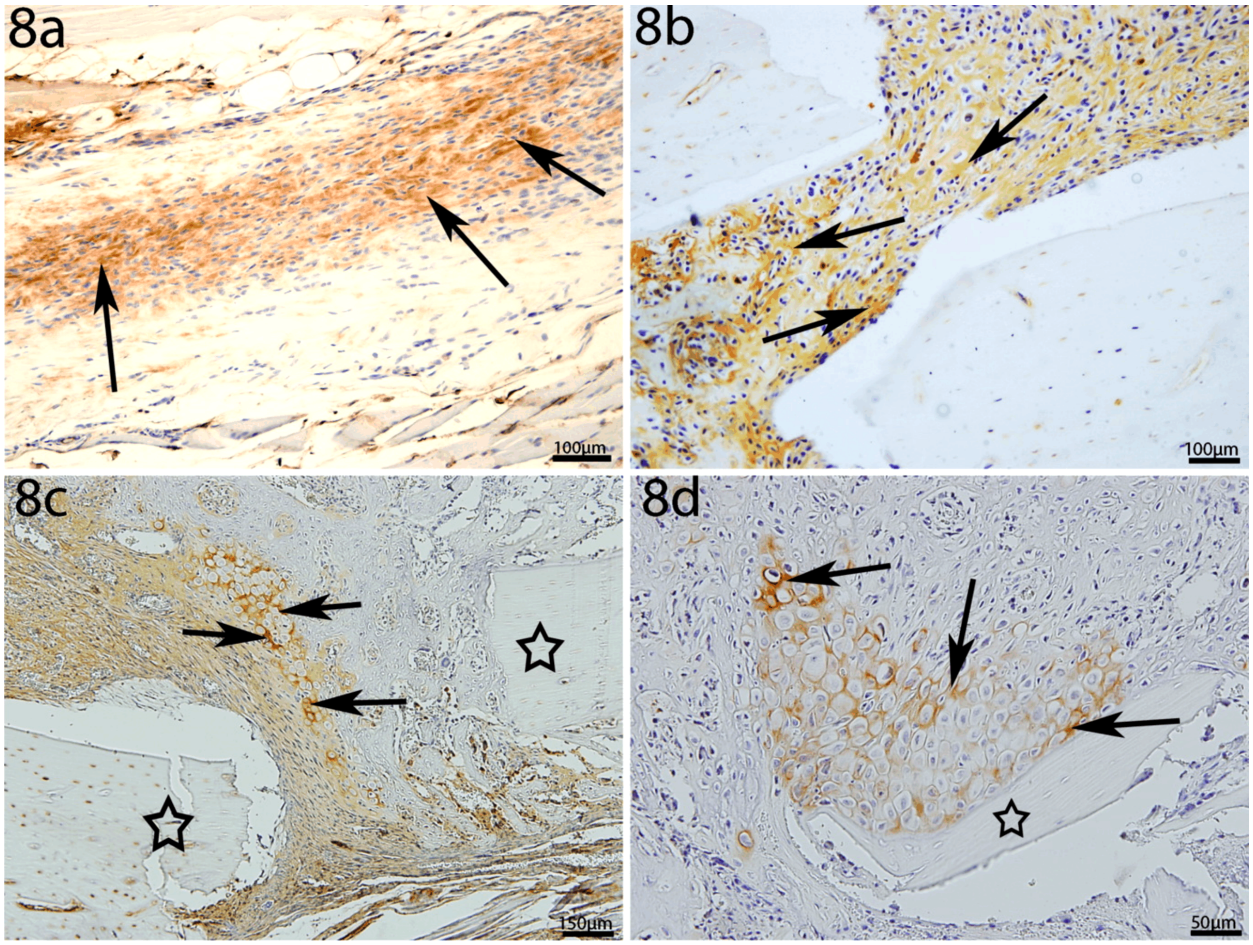

Figure 8 – ***Photomicrographs of transverse bone fracture sections, showing immunoreaction for coll-II: (a) At 96 hours post-injury, immunoreaction was visible in the periosteum (arrows); (b) At 144 hours post-injury, an intercellular immunoreaction (arrows) was observed in the central region of the fracture; (c) At 192 hours post-injury, labeling was observed in the ECM of a small group of chondrocytes in the central region (arrows) between bone fragments (stars); (d) At 240 hours post-injury, coll-II was identified in the pericellular matrix of hypertrophic chondrocytes near the bone fragment (star). coll-II: Type II collagen; ECM: Extracellular matrix.***

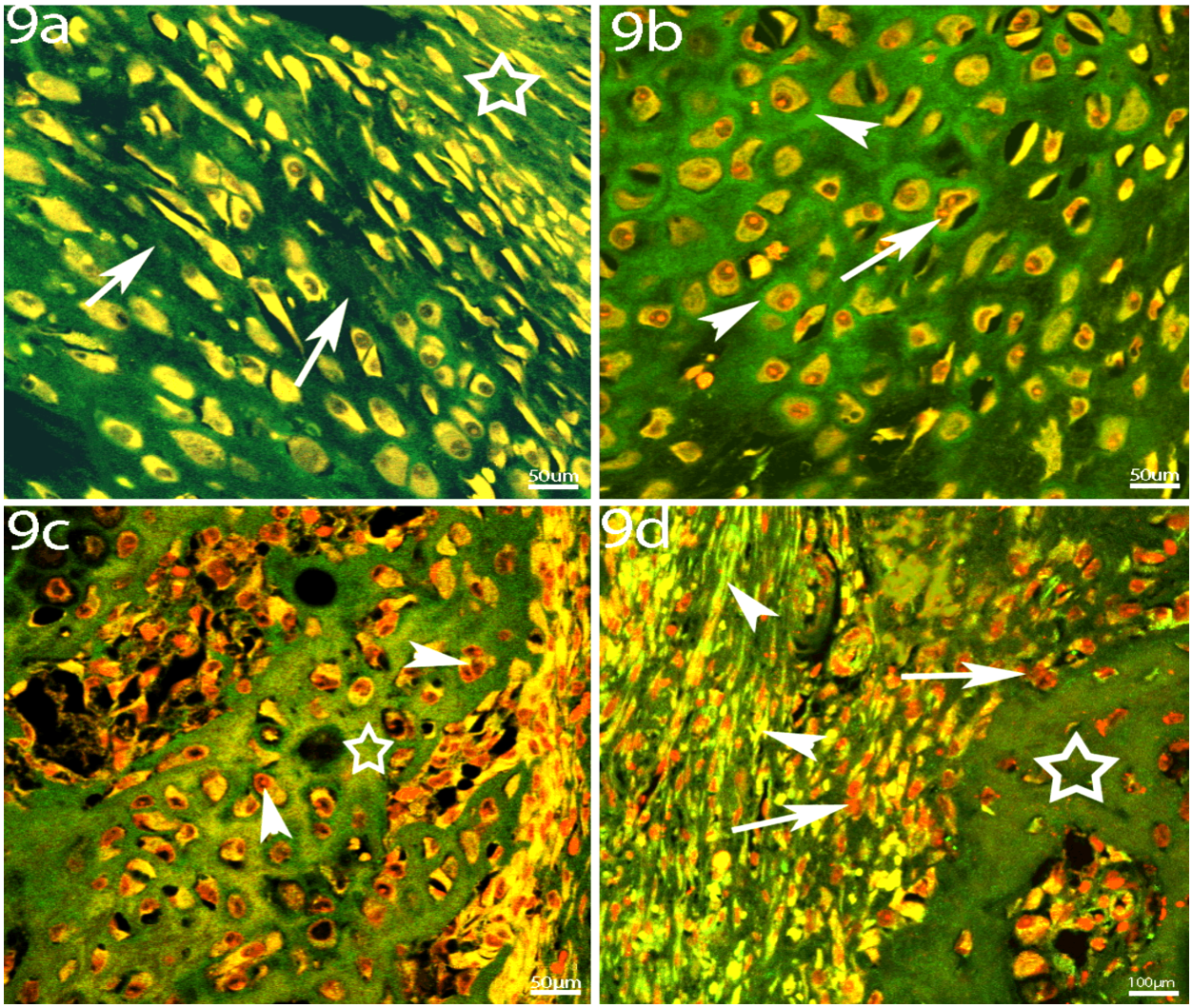

Figure 9 – ***Photomicrographs of transverse bone fracture sections, showing immunofluorescence for coll-II and double staining for procoll-I (red) and coll-I (green): (a) At 96 hours post-injury, a green plot of coll-II was observed in the ECM (arrows) and in the periosteal layer (star); (b) At 144 hours post-injury, the highest expression of coll-II was observed in the pericellular region (arrowheads) – isogenic cell groups (arrow) indicates a chondrogenic area; (c) At 192 hours post-injury, a few cells, including a group of isogenic cells (arrowheads) expressed procoll-I – coll-I was observed in the ECM (star); (d) At 240 hours post-injury, the coll-I distribution pattern was more homogeneous in the ECM in the central region of the fracture, as well as in nearly every osteogenic region (arrowheads) – procoll-I was also identified intracellularly (arrows) near the bone fragment (star). procoll-I: Type I procollagen; coll-I: Type I collagen; coll-II: Type II collagen; ECM: Extracellular matrix.***

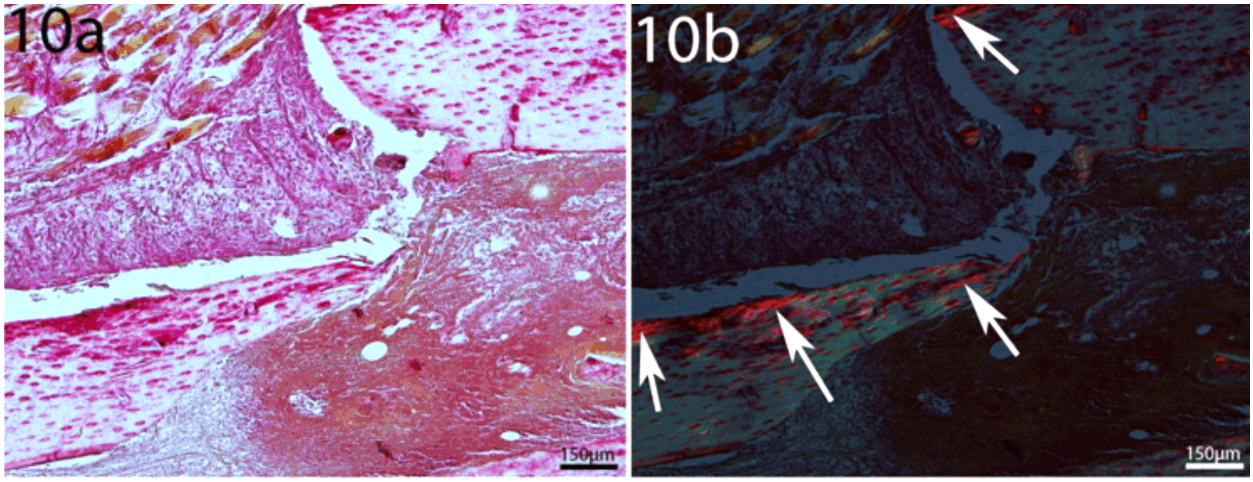

Figure 10 – ***Photomicrographs of transverse bone fracture sections showing staining for T-coll visualized under polarized light: (a and b) At 96 hours post-injury, small amounts of collagen fibers were observed in the central region of the fracture (arrows). T-coll: Total collagen.***

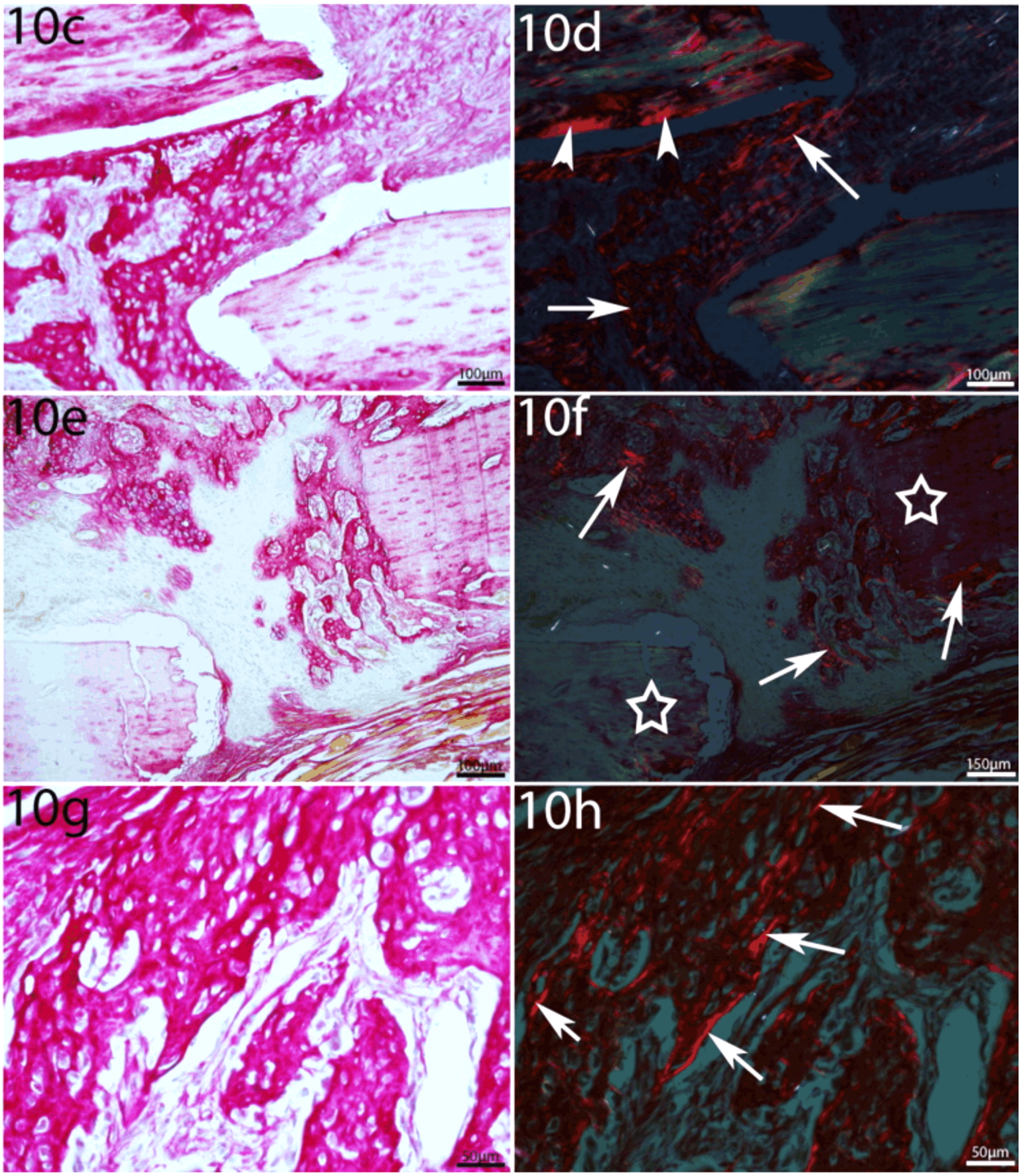

Figure 10 (continued) – ***Photomicrographs of transverse bone fracture sections showing staining for T-coll visualized under polarized light: (c and d) At 144 hours post-injury, staining was observed in the central region of the fracture (arrows) and at the end of the bone fragment (arrowheads); (e and f) At 192 hours post-injury, T-coll was identified in a small area in the central region of the fracture, as well as at the ends of bone fragments (stars); (g and h) At 240 hours post-injury, T-coll was observed in the ECM of the new bone (arrows). T-coll: Total collagen; ECM: Extracellular matrix.***

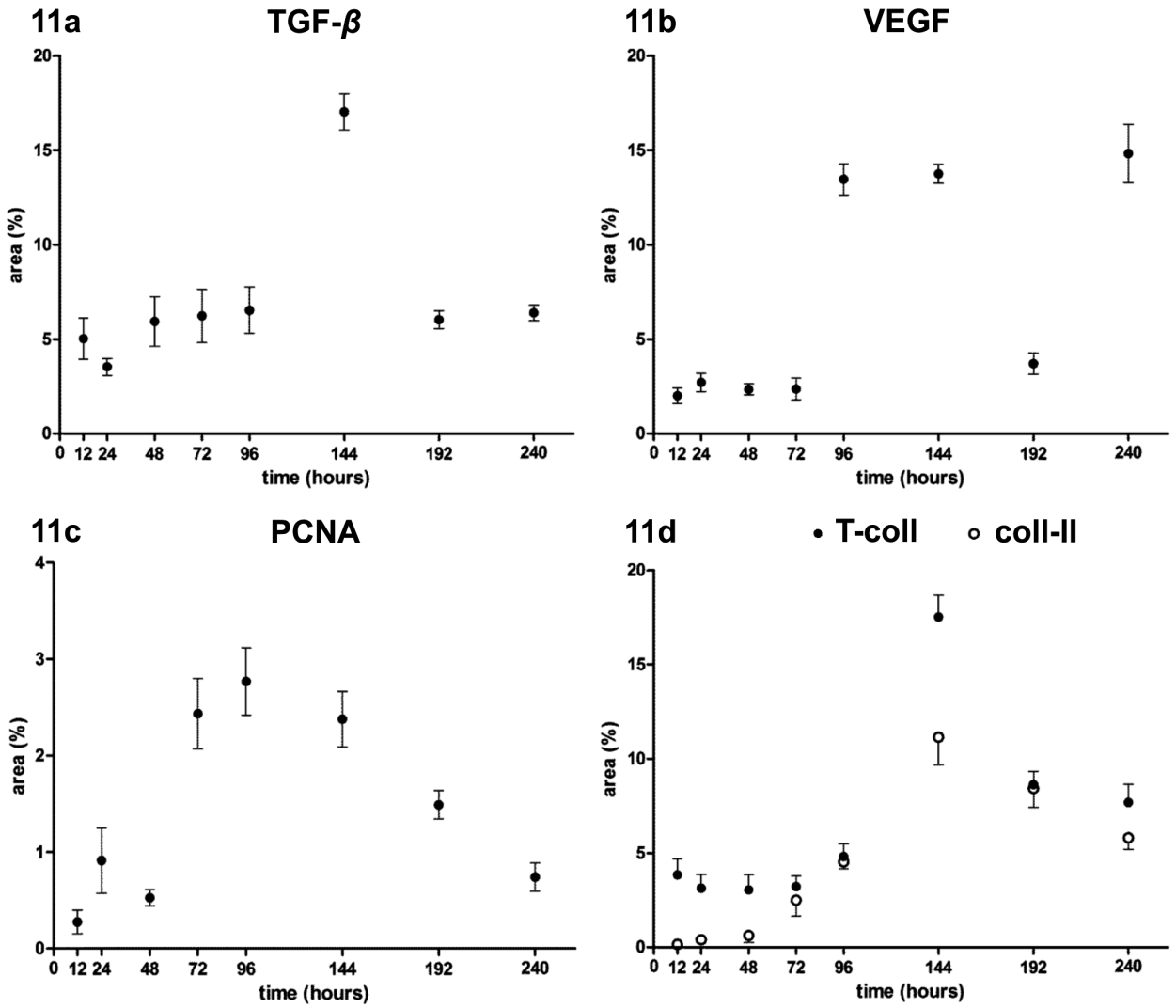

Figure 11 – ***Morphometric results. Expression peak (per area) of each ECM component at different time points after injury with their respective standard error bars. In d, black and clear spots represent T-coll and coll-II, respectively. ECM: Extracellular matrix; TGF-β: Transforming growth factor-beta; VEGF: Vascular endothelial growth factor; PCNA: Proliferating cell nuclear antigen; T-coll: Total collagen; coll-II: Type II collagen.***

Discussion

Fracture healing is a unique postnatal repair process in which both endochondral and intramembranous bone formation can be reproducibly initiated in a definable temporal sequence [18]. In our study, we established a standardized experimental model in rats [14] using a standard guillotine method [19], with some modifications to minimize damage to soft tissues. Previous evidence has demonstrated the important role of adjacent soft tissues, such as periosteum, in fracture healing [20]. This is one of the reasons for standardizing the experimental fracture induction and subsequently observing the healing process.

Of the induced fractures, 68% were transverse fractures, showing that the apparatus used in this study produces a standard type of experimental fracture and is appropriate for studies of cells and ECM components.

Fracture repair is a complex process that involves timed cellular recruitment, gene expression, and synthesis of compounds that regenerate the tissue to restore mechanical integrity and therefore the function of injured bone [21]. HE-stained histological sections obtained between 12 hours and 240 hours post-injury showed the different stages of the healing process [22], including hematoma formation and the immediate response to injury, intramembranous bone formation, chondrogenesis, and endochondral ossification. We did not observe the last phase of bone remodeling. Masson's trichrome staining distinguished cells of the surrounding connective tissue, allowing identification of chondrogenesis and osteogenesis, the two main phases of the healing process investigated in this study.

Previous studies have suggested that TGF-β is involved in the initial formation of the callus [23] and is produced by osteoblasts and chondrocytes in the later phases of healing, increasing the proliferation of these cells, as well as of mesenchymal cells and pre-osteoblasts. In addition, some investigators have reported high TGF-β expression during chondrogenesis and endochondral bone formation, with an initial peak in messenger ribonucleic acid (mRNA) levels detected around day 6 post-fracture, followed by

a nadir at day 10 that correlates with a peak in coll-II expression. According to our morphometric analysis, TGF-β expression began at 12 hours (when it was mostly localized in the fracture hematoma), peaked at 144 hours (six days), and declined gradually until 240 hours after injury, suggesting that TGF-β expression plays an important role in the chondrogenic and osteogenic phases of bone healing and consequently in controlling bone architecture and bone mass. Our results corroborate those of previous studies that showed a constant TGF-β expression throughout fracture consolidation [18, 22, 23].

Another important ECM component, VEGF, has been shown to play a central role in angiogenesis for endochondral bone formation. Osteoblasts express high levels of VEGF and are considered one of the main regulators of angiogenesis in fracture repair [24]. VEGF is also involved in conversion of the cartilaginous callus to a bone callus in the healing process, wherein chondrocytes undergo differentiation into osteoblasts to synthesize a calcified matrix [9]. While some studies have shown that VEGF is highly expressed during the early phases of bone healing [24], others have reported that VEGF is expressed throughout the chondrogenic phase, reaching maximal expression levels during the late phases of cartilage calcification, after chondrocyte apoptosis and resorption initiation [10, 25]. We found that VEGF expression was constant from 12 hours until 72 hours post-injury and then reached a peak in the chondrogenic phase at 96 hours and 144 hours. Following a significant decrease after 192 hours, VEGF expression reached another peak at 240 hours. These results suggest that VEGF plays a role in all stages of bone healing, including that of intense mesenchymal stem cell recruitment to promote bone regeneration. We hypothesize that VEGF enhanced angiogenesis, but we did not investigate its possible involvement in the conversion of cartilage cells into osteogenic cells.

Similar to previous reports [26], the PCNA distribution pattern observed in this study suggests that after proliferation, periosteal cells migrate to chondrogenic and osteogenic areas where they can differentiate into chondroblasts and osteoblasts, respectively. PCNA expression reached a peak at 96 hours post-injury, preceding the expression peak of coll-II, which suggests that chondrogenic differentiation occurs during this phase. Our results are consistent with those of studies that have shown high proliferative activity in the soft tissue in the early phase of tibial fracture healing and less intense activity in the osteogenic layer [27].

Fibrillar collagen (>90%) constitutes the main building material of the soft and hard calluses formed during fracture healing [28]. We observed peak coll-II expression at the chondrogenic phase, 144 hours post-injury. Its expression decreased between 192 hours and 240 hours, suggesting osteogenic formation. Although we observed reduced amounts of coll-II at early time points, immunoreaction was identified in the periosteal ECM near the fracture area containing cells, suggesting that some periosteal cells were committed to the chondrocyte lineage. In addition, we did not observe differences between T-coll and coll-II expression in any of the bone healing stages studied, suggesting that cells from the periosteum can differentiate into chondrocytes or osteoblasts. Our results agree with those of previously published studies that showed immature and mature chondrocytes, hypertrophic chondrocytes, and endochondral ossification in specific regions of the callus. According to the immunohistochemistry results of that study, coll-II was first observed in immature chondrocytes on day 5, and intense signals were identified in the fracture cartilage on days 7 and 9. Coll-II signals decreased with endochondral ossification progression [29].

Considering that only osteoblasts and osteocytes express coll-I mRNA [30], we used immunofluorescence double staining for coll-I and procoll-I to distinguish the differentiation of osteoblastic cells from mature chondrocytes, which express coll-II [31]. From 96 hours to 144 hours post-injury, coll-I staining was observed in the ECM, and procoll-I was intracellular and adjacent to the centre of the fracture line, as we observed a layer of the periosteum containing undifferentiated cells. Furthermore, the presence of small lacunae at the same site suggests initial formation of an osteogenic area. Groups of isogenic cells with characteristics of mature chondrocytes were also observed. These results suggest that undifferentiated cells express both coll-I and coll-II in the area adjacent to the centre of the fracture and agree with those of a previous study that showed that some areas in regenerating tissues have morphological characteristics of both bone and cartilage, in which cells express both coll-I and coll-II mRNA, which characterizes them as areas of chondroid bone [32].

In the late phase of bone healing, *i.e.*, 240 hours post-injury, we observed characteristics of osteogenesis in the central region of the fracture, given that coll-I and procoll-I were highly expressed in the ECM. Considering that the coll-II expression peak preceded that of coll-I (as observed in the morphometric analysis), we suggest that although cells of the periosteal layer at the edges of the fracture expressed both coll-I and coll-II (with a higher prevalence of coll-II) in the initial stages of healing, in later stages, hypertrophic chondrocytes were modulated by mineralized ECM-containing coll-I. Given that procoll-I was expressed intracellularly, we assume that procoll-I-expressing cells were committed to deposit coll-I to the ECM and therefore to differentiate into osteoblasts. Unlike other authors [9], we suggest that a lineage of procoll-I-expressing stem cells is already committed to the formation of osteoblasts in the osteogenic area and, likewise, coll-II-expressing cells in chondrogenic areas are committed to the cartilage lineage.

Although bone repair processes have been widely investigated in an attempt to create new therapies to accelerate fracture healing, in this work, we observed that a number of molecular mediators and cells interact through different pathways, and we examined the role that each one plays mainly in the chondrogenic and osteogenic phases of the bone regeneration process.

The mechanisms of action of cells and ECM components involved many local and systemic factors,

evidenced by the studies cited here. However, our results revealed that larger peaks of the studied components were between the chondrogenic and osteogenic phases, suggesting the most important phase of the differentiation precursor cell in chondroblasts and osteoblasts. Any failure that interferes in this regeneration phase can lead to the delay of bone fracture consolidation or even non-consolidation.

Conclusions

The results suggest that the spatiotemporal expression of ECM components during the chondrogenic and osteogenic phases of bone healing depends on several combined and orchestrated factors, such as VEGF, TGF-β, PCNA, and collagen types I and II. Disruption of the homeostasis between these factors can impede consolidation or lead to fracture healing problems. A better understanding of the intricate interactions between these molecules will shed light on the basic biology of bone formation and healing and thus contribute to the development of more effective therapeutic strategies to improve bone healing.

Conflict of interests

The authors declare no conflict of interests.

Acknowledgments

Financial support was provided by the following Groups: FAPERJ – Support Foundation Research of Rio de Janeiro; CAPES – Coordination of Personnel Improvement of Higher Education; CNPq – National Council for Scientific and Technological Development; UERJ – State University of Rio de Janeiro, Brazil.

References

[1] Gemalmaz A, Discigil G, Sensoy N, Basak O. Identifying osteoporosis in a primary care setting with quantitative ultrasound: relationship to anthropometric and lifestyle factors. J Bone Miner Metab, 2007, 25(3):184–192.

[2] Lee YK, Yoon BH, Koo KH. Epidemiology of osteoporosis and osteoporotic fractures in South Korea. Endocrinol Metab (Seoul), 2013, 28(2):90–93.

[3] Steingrimsdottir L, Halldorsson TI, Siggeirsdottir K, Cotch MF, Einarsdottir BO, Eiriksdottir G, Sigurdsson S, Launer LJ, Harris TB, Gudnason V, Sigurdsson G. Hip fractures and bone mineral density in the elderly – importance of serum 25-hydroxyvitamin D. PLoS One, 2014, 9(3):e91122.

[4] Gupta HS, Zioupos P. Fracture of bone tissue: the 'hows' and the 'whys'. Med Eng Phys, 2008, 30(10):1209–1226.

[5] Mognetti B, Marino S, Barberis A, Martin AS, Bala Y, Di Carlo F, Boivin G, Barbos MP. Experimental stimulation of bone healing with teriparatide: histomorphometric and microhardness analysis in a mouse model of closed fracture. Calcif Tissue Int, 2011, 89(2):163–171.

[6] Zimmermann G, Schmeckenbecher KHK, Boeuf S, Weiss S, Bock R, Moghaddam A, Richter W. Differential gene expression analysis in fracture callus of patients with regular and failed bone healing. Injury, 2012, 43(3):347–356.

[7] Mehrotra M, Williams CR, Ogawa M, LaRue AC. Hematopoietic stem cells give rise to osteo-chondrogenic cells. Blood Cells Mol Dis, 2013, 50(1):41–49.

[8] Zhang X, Schwarz EM, Young DA, Puzas JE, Rosier RN, O'Keefe RJ. Cyclooxygenase-2 regulates mesenchymal cell differentiation into the osteoblast lineage and is critically involved in bone repair. J Clin Invest, 2002, 109(11):1405–1415.

[9] Scammell BE, Roach HI. A new role for the chondrocyte in fracture repair: endochondral ossification includes direct bone formation by former chondrocytes. J Bone Miner Res, 1996, 11(6):737–745.

[10] Ai-Aql ZS, Alagl AS, Graves DT, Gerstenfeld LC, Einhorn TA. Molecular mechanisms controlling bone formation during fracture healing and distraction osteogenesis. J Dent Res, 2008, 87(2):107–118.

[11] Vardaxis NJ, Brans TA, Boon ME, Kreis RW, Marres LM. Confocal laser scanning microscopy of porcine skin: implications for human wound healing studies. J Anat, 1997, 190(Pt 4):601–611.

[12] Nikonova A, Harrison AJ. A simple way to model wires used in rig fixators: analysis of the wire stiffness effect on overall fixator stiffness. Proc Inst Mech Eng H, 2005, 219(1):31–42.

[13] Whelan DB, Bhandari M, Stephen D, Kreder H, McKee MD, Zdero R, Schemitsch EH. Development of the radiographic union score for tibial fractures for the assessment of tibial fracture healing after intramedullary fixation. J Trauma, 2010, 68(3):629–632.

[14] An Y, Friedman RJ, Parent T, Draughn RA. Production of a standard closed fracture in the rat tibia. J Orthop Trauma, 1994, 8(2):111–115.

[15] Müller ME, Nazarian S, Koch P, Schatzker J. The comprehensive classification of fractures of long bones. 1st edition, Springer-Verlag, Berlin–Heidelberg–New York, 1994, 148–156.

[16] Karnovsky MJ. A formaldehyde-glutaraldehyde fixative of high osmolality for use in electron microscopy. J Cell Biol, 1965, 27(2):137–138A.

[17] Sugimoto H, Mundel TM, Sund M, Xie L, Cosgrove D, Kalluri R. Bone-marrow-derived stem cells repair basement membrane collagen defects and reverse genetic kidney disease. Proc Natl Acad Sci U S A, 2006, 103(19):7321–7326.

[18] Cho TJ, Gerstenfeld LC, Einhorn TA. Differential temporal expression of members of the transforming growth factor beta superfamily during murine fracture healing. J Bone Miner Res, 2002, 17(3):513–520.

[19] Bonnarens F, Einhorn TA. Production of a standard closed fracture in laboratory animal bone. J Orthop Res, 1984, 2(1): 97–101.

[20] Neagu TP, Ţigliş M, Cocoloş I, Jecan CR. The relationship between periosteum and fracture healing. Rom J Morphol Embryol, 2016, 57(4):1215–1220.

[21] Komatsu DE, Warden SJ. The control of fracture healing and its therapeutic targeting: improving upon nature. J Cell Biochem, 2010, 109(2):302–311.

[22] Barnes GL, Kostenuik PJ, Gerstenfeld LC, Einhorn TA. Growth factor regulation of fracture repair. J Bone Miner Res, 1999, 14(11):1805–1815.

[23] Bolander ME. Regulation of fracture repair by growth factors. Proc Soc Exp Biol Med, 1992, 200(2):165–170.

[24] Hankenson KD, Dishowitz M, Gray C, Schenker M. Angiogenesis in bone regeneration. Injury, 2011, 42(6):556–561.

[25] Allerstorfer D, Longato S, Schwarze C, Fischer-Colbrie R, Hayman AR, Blumer MJF. VEGF and its role in the early development of the long bone epiphysis. J Anat, 2010, 216(5):611–624.

[26] Li G, White G, Connolly C, Marsh D. Cell proliferation and apoptosis during fracture healing. J Bone Min Res, 2002, 17(5):791–799.

[27] Wildemann B, Schmidmaier G, Ordel S, Stange R, Haas NP, Raschke M. Cell proliferation and differentiation during fracture healing are influenced by locally applied IGF-I and TGF-beta1: comparison of two proliferation markers, PCNA and BrdU. J Biomed Mater Res B Appl Biomater, 2003, 65(1): 150–156.

[28] Galvis L, Mehta M, Mašić A, Dunlop JWC, Duda G, Fratzl P. Collagen orientation during early stages of bone fracture healing investigated by polarized Raman imaging. In: Champion PM, Ziegler LD (eds). XXII International Conference on Raman Spectroscopy. American Institute of Physics, Boston, MA, USA, 2010, 406–407.

[29] Sakano S, Zhu Y, Sandell LJ. Cartilage-derived retinoic acid-sensitive protein and type II collagen expression during fracture healing are potential targets for Sox9 regulation. J Bone Miner Res, 1999, 14(11):1891–1901.

[30] Li G, Virdi AS, Ashhurst DE, Simpson AHRW, Triffitt JT. Tissues formed during distraction osteogenesis in the rabbit are determined by the distraction rate: localization of the cells that express the mRNAs and the distribution of types I and II collagens. Cell Biol Int, 2000, 24(1):25–33.

[31] Lane JM, Suda M, von der Mark K, Timpl R. Immuno-fluorescent localization of structural collagen types in endochondral fracture repair. J Orthop Res, 1983, 4(3):318–329.

[32] Beresford WA. Chondroid bone, secondary cartilage, and metaplasia. 1st edition, Urban & Schwarzenberg, Baltimore–Munich, 1981, 381–442.

Corresponding author

Moyses Messias Souza de Sant'Anna, MSc, PhD, Laboratory of Ultrastructure and Tissue Biology, Department of Histology and Embryology, Biomedical Center, Institute of Biology, State University of Rio de Janeiro (UERJ), Rua Quiririm, 902. Rua B, Casa 34 – Vila Valqueire – CEP: 21.330-650, Rio de Janeiro, Brazil; Phone 55(21) 24894587, Fax 55(21) 25876511, e-mail: moysa2000@yahoo.com

Received: May 8, 2017

Accepted: January 24, 2018